Journal for ImmunoTherapy of Cancer

Fc-competent TIGITx4-1BB bispecific antibody exerts potent long-lasting antitumor activity by potentiating CD8$^+$ T cell activity and Fcγ receptor-mediated modulation of the tumor microenvironment

Wonjun Son,[1] Yangsoon Lee,[1] Yelim Park,[1] Kyeong-Su Park,[1] Sora Kim,[1] Hyunseong Youn,[1] Arim Seo,[2] Byungje Sung,[3] Sang Hoon Lee,[4] Jonghwa Won [1]

To cite: Son W, Lee Y, Park Y, *et al*. Fc-competent TIGITx4-1BB bispecific antibody exerts potent long-lasting antitumor activity by potentiating CD8$^+$ T cell activity and Fcγ receptor-mediated modulation of the tumor microenvironment. *Journal for ImmunoTherapy of Cancer* 2025;**13**:e010728. doi:10.1136/jitc-2024-010728

► Additional supplemental material is published online only. To view, please visit the journal online (https://doi.org/10.1136/jitc-2024-010728).

Accepted 04 February 2025

[1]Oncology Discovery, ABL Bio Inc, Seongnam, Korea (the Republic of)
[2]Quality Control, ABL Bio Inc, Seongnam, Korea (the Republic of)
[3]Analytics, ABL Bio Inc, Seongnam, Korea (the Republic of)
[4]ABL Bio Inc, Seongnam, Korea (the Republic of)

Correspondence to
Dr Jonghwa Won;
jonghwa.won@ablbio.com

ABSTRACT

Background TIGIT was identified as a target immune checkpoint for overcoming resistance to PD-(L)1-blocking antibodies. However, the clinical efficacies of TIGIT antibodies were moderate in monotherapy and mixed in combination with PD-(L)1 antibodies. 4-1BB, a strong inducible costimulatory receptor, is another attractive target in antitumor therapeutics. This study investigated whether ABL112, an Fc-competent bispecific antibody targeting TIGIT and 4-1BB (TIGITx4-1BB), would enhance antitumor activity via Fcγ receptor (FcγR)-mediated macrophage activation and antibody-dependent cell-mediated functions.

Methods TIGIT-dependent 4-1BB activation and TIGIT-blocking activity were assessed using reporter Jurkat T cell lines expressing 4-1BB and TIGIT, respectively. In vivo antitumor activity was confirmed in h4-1BB knock-in mice. The main immune cell subsets associated with the antitumor activity of ABL112 were identified using antibodies for depleting specific immune cell subtypes or FcγR-blocking antibodies. The effects of a combined pembrolizumab or atezolizumab treatment with ABL112 were assessed in two mouse models with different genetic backgrounds. Statistical analysis was performed using one-way or two-way analysis of variance (ANOVA) with Dunnett's multiple-comparison test or one-way ANOVA with Fisher's multiple-comparison test.

Results ABL112 restored T cell activity by blocking TIGIT–CD155 interactions, based on a TIGIT blockade reporter assay. ABL112, an Fc-competent TIGITx4-1BB bispecific antibody, showed strong FcγRI-dependent 4-1BB activation along with TIGIT-dependent 4-1BB activation. In H22 tumor models expressing high levels of endogenous CD155, both ABL112 and parent TIGIT single-domain Ab showed potent tumor-suppressive activity; however, only ABL112 exerted long-lasting antitumor activity. ABL112 induced a marked decrease in Treg numbers, while augmenting the absolute number of CD8$^+$ T cells and proportion of CD226$^+$ CD8$^+$ T cells. The expressions of CXCL10, CXCL11, IFN-γ, and TNF-α increased, indicating myeloid cell activation and potential modification of the tumor microenvironment to an inflammatory phenotype. ABL112 not only showed outstanding antitumor activity as a monotherapy, but also showed synergistic effects with PD-(L)1 mAb compared with the combined TIGIT–PD-(L)1 mAb treatments.

Conclusions Through multiple mechanisms of action, ABL112 exerted potent tumor-killing activity and immune memory response alone or in combination with anti-PD-(L)1 therapies, representing a promising new cancer treatment strategy.

WHAT IS ALREADY KNOWN ON THIS TOPIC

⇒ Although TIGIT was identified as a marker of resistance against PD-(L)1 antibodies, the TIGIT antibody has shown limited efficacy as monotherapy or in combination with PD-(L)1 antibodies.

WHAT THIS STUDY ADDS

⇒ Via various functional mechanisms, including TIGIT-dependent 4-1BB activation and FcγR-binding activity, a TIGITx4-1BB bispecific antibody stimulated the innate as well as adaptive immune responses.

HOW THIS STUDY MIGHT AFFECT RESEARCH, PRACTICE OR POLICY

⇒ The outstanding antitumor efficacy in combination with PD-(L)1 antibodies stemmed from T cell activation and alterations in the tumor microenvironment involving Treg depletion and myeloid cell activation. The findings can inform the development of antitumor immunotherapies in hematological malignancies and solid tumors.

BACKGROUND

T cell immunoreceptor with Ig and ITIM domains (TIGIT) is an inhibitory immune

checkpoint receptor suppressing T cell activation by interacting with the poliovirus receptor (also known as CD155) expressed in dendritic cells, macrophages, and tumor cells. Like CTLA-4, which competes with CD28 for CD80/86 binding,[1–4] TIGIT competes with its counter-receptor CD226, a costimulatory receptor, for binding to CD155. TIGIT expression is induced after T cell activation and regulates T cell activity by disrupting CD226–CD155 interactions and triggering T cell inhibitory signaling.[2 3] TIGIT is a promising target for immune checkpoint inhibitors (ICIs) beyond PD-(L)1 inhibitors.[5] However, anti-TIGIT antibody monotherapy showed limited clinical efficacy, and combination therapy with PD-(L)1 or chemotherapy exhibited somewhat mixed results.[6 7] In the CITYSCAPE phase II study of advanced non-small-cell lung cancer (NSCLC), the combination of tiragolumab (600 mg) plus atezolizumab (1200 mg) showed increased efficacy compared with placebo plus atezolizumab (objective response rate (ORR): 31.3% vs 16.2%; median progression-free survival (PFS): 5.4 vs 3.6 months).[8] However, in the phase III SKYSCRAPER-01 study of PD-L1^{high} metastatic NSCLC, the combination of tiragolumab and atezolizumab did not meet the primary endpoint of PFS and awaits further clinical assessment.[7] Antibodies targeting TIGIT have different mechanisms with either an 'enabled' Fc function (able to interact with various Fc receptors) or 'silent' Fc function (mutated to prevent interaction with Fc receptors).[9 10] Compared with tiragolumab, which has the wild-type Fc, domvanalimab is a Fc-null anti-TIGIT antibody. The phase II ARC-7 trial showed that the combination of domvanalimab (15 mg/kg) and zimberelimab (anti-PD-1 antibody, 360 mg) improved clinical outcomes (ORR: 41% vs 27%; median PFS: 12.0 vs 5.4 months) compared with zimberelimab alone in patients with PD-L1^{high} NSCLC.[11] In the phase II EDGE-Gastric study, the combination of domvanalimab (1600 mg), zimberelimab (480 mg), and FOLFOX produced encouraging preliminary results (ORR: 59%).[12]

4-1BB is a potent costimulatory immune receptor of the TNF receptor superfamily and is expressed in response to T cell activation.[13 14] Along with T cell antigen receptor signaling, 4-1BB activation potentiates T cell activation and proliferation and prevents activation-induced cell death.[15] Although 4-1BB plays pivotal roles in the protective immune response, the early development of 4-1BB agonists was unsuccessful. Strong and unconditional 4-1BB activation by urelumab developed by BMS led to severe liver toxicity and discontinuation of the trial.[16] In contrast, utomilumab, a 4-1BB agonist developed by Pfizer, was discontinued due to its low clinical efficacy.[17] To avoid liver toxicity arising from unconditional 4-1BB activation while maintaining efficacy, conditional 4-1BB agonists are being considered. CTX-471 and ADG106 containing the 4-1BB ligand non-competitive epitope is dependent on Fc receptor (FcγR) engagement for 4-1BB activation, while STA551 activates 4-1BB in the presence of extracellular ATP in tumor environments.[18–21] AGEN-2373 activated 4-1BB via FcγRIIB crosslinking and simultaneously depleted 4-1BB^{+} regulatory T cells via antibody-dependent cell-mediated cytotoxicity (ADCC) and antibody-dependent cell-mediated phagocytosis (ADCP).[22 23] 4-1BB activity can be concentrated to the tumor microenvironment (TME) by leveraging bispecific antibodies with tumor-associated antigen (TAA)-dependent activities. In our previous study, ABL503 (TJ-L14B, PD-L1×4–1BB)[24] and ABL111 (TJ-CD4B, Claudin 18.2×4–1BB)[25] induced 4-1BB activation in a TAA-dependent manner and showed good efficacy with manageable toxicity.

In this study, we hypothesized that linking anti-4-1BB single-chain fragment variable (scFv) to the C-terminal ends of Fc-enabled TIGIT single-domain antibody (sdAb) would generate novel functions. TIGITx4-1BB bispecific antibody (BsAb) could restore T cell activity by blocking TIGIT–CD155 interactions and inducing 4-1BB signaling in a TIGIT expression-dependent manner. By retaining Fc activity, the BsAb may induce FcγR-dependent 4-1BB activation, 4-1BB/TIGIT-dependent FcγR activation, and cell-mediated depletion of 4-1BB overexpressing regulatory T cells (Tregs). Our findings suggested that an Fc-competent TIGITx4-1BB BsAb (ABL112) exerts potent and long-lasting antitumor activity through TIGIT blockade, FcγR-mediated TME activation, and 4-1BB-mediated immune memory.

METHODS

Cell lines and cell culture

Jurkat T cells overexpressing human 4-1BB (Jurkat/h4-1BB) and CHO-K1 cells overexpressing human FcγRIIb (CHO-K1/FcgRIIb) were purchased from Promega (Madison, Wisconsin, USA). CHO-K1-overexpressing human TIGIT (CHO-K1/TIGIT), human FcγRI (CHO-K1/FcγRI), and human FcγRIIIa (CHO-K1/FcγRIIIa) were purchased from GenScript (Piscataway, New Jersey, USA). CT26 and H22 cells were purchased from American Type Culture Collection (ATCC; Manassas, Virginia, USA) and China Center for Type Culture Collection (CCTCC; Wuhan, China), respectively. CT26 cells overexpressing human PD-L1 (CT26/hPD-L1) were obtained from GemPharmatech (Nanjing, China). MC38 cells were purchased from Shunran Shanghai Biological Technology (Shanghai, China). Jurkat/h4-1BB cells were maintained in RPMI 1640 (Gibco, Waltham, Massachusetts, USA) supplemented with 10% fetal bovine serum (FBS; Gibco), 500 µg/mL hygromycin B (Gibco), 800 µg/mL G418 sulfate (Gibco), 1 mM sodium pyruvate (Gibco), and 0.1 mM MEM non-essential amino acids (Gibco). CHO-K1/TIGIT cells were maintained in F-12K (ATCC) supplemented with 10% FBS (Gibco) and 6 µg/mL puromycin (Gibco). CHO-K1/FcγRI cells were maintained in F-12K supplemented with 10% FBS, 300 µg/mL hygromycin B, and 8 µg/mL puromycin. CHO-K1/FcγRIIIa cells were maintained in F-12K supplemented with 10% FBS, 200 µg/mL hygromycin B, and 8 µg/mL puromycin. CT26 cells and H22 cells

were maintained in RPMI 1640 supplemented with 10% FBS and 1% penicillin/streptomycin (P/S; AMRESCO; Radnor, Pennsylvania, USA). CT26/hPD-L1 cells were maintained in RPMI 1640 supplemented with 10% FBS, 200 µg/mL G418 sulfate (Gibco), and 1% P/S. MC38 cells were maintained in Dulbecco Modified Eagle Medium (Gibco) supplemented with 10% FBS. All cell lines were maintained at 37°C in 5% CO_2.

TIGIT blockade and 4-1BB activation reporter assay

TIGIT-blocking activity was determined in duplicate using a TIGIT/CD155 blockade bioassay (Promega) according to the manufacturer's protocol and repeated twice. Briefly, CD155 aAPC/CHO-K1 cells (4×10^4 cells/well) were incubated with TIGIT effector cells (1.5×10^5 cells/well) in the presence of TIGIT-blocking antibodies for 6 hours at 37°C in a 5% CO_2 humidified incubator. After 6 hours of incubation, 75 µL of BIO-GLO reagent was added per well to the assay plate. After 5 min, luminescence was quantified using a microplate reader (PHERAstar FS, BMG LABTECH, Ortenberg, Germany). Four-parameter logistic curve analysis was performed using GraphPad Prism software V.10.0.1 (GraphPad Software Inc, San Diego, California, USA).

To determine 4-1BB activation, GloResponse NF-κB-luc2/4-1BB Jurkat cells (5×10^4 cells, used as effector cells; Promega) were incubated in duplicate with CHO-K1 cells expressing human TIGIT, FcγRI, FcγRIIb, or FcγRIIIa (2.5×10^4) in the presence of antibodies at 37°C for 6 hours in a 5% CO_2 humidified incubator. After incubation, 75 µL of Bio-GLO Reagent was added to each well for 5 min before the plate was assessed using the microplate reader. The experiments were repeated twice. The four-parameter logistic curve was evaluated using GraphPad Prism V.10.0.1 (GraphPad Software Inc.).

In vivo tumor growth inhibition and re-challenge study

BALB/c-hCD137 (h4-1BB) knock-in mice (BALB/cJGpt-Tnfrsf9$^{em1Cin(hTNFRSF9)}$/Gpt) were supplied by GemPharmatech. The protocols and any amendments involving the care and use of animals in this experiment were reviewed and approved by the Institutional Animal Care and Use Committee (IACUC) of GemPharmatech (GPTAP20221010-6/GPTAP20230214-2/GPTAP20230627-4/GPTAP20231030-2). To establish a CT26 model, 6–8 week-old female BALB/c-h4-1BB mice were injected subcutaneously with CT26 tumor cells (5×10^5 cells/0.1 mL/mouse) in the lower right flank. One and a half times the number of mice were inoculated with CT26 tumor cells, and mice with tumors showing a deviation less than one-third of the mean tumor volume were used for the study. When the mean tumor volume reached ~80 mm^3, mice were assigned to their respective treatment group and administered intraperitoneally with hIgG1 (isotype control, 3 mg/kg), parent anti-TIGIT sdAb (1.6 mg/kg), ABL112 (2.6 mg/kg), COM-902 analog (3 mg/kg), and urelumab (3 mg/kg) two times per week for a total of six times. The dosing volume was adjusted based on the body weight (10 µL/g). Each group consisted of 8 mice, and a total of 24 mice were used for the study. The tumor volume (mm^3, 0.5 × length × $width^2$) and body weight were recorded two times per week. Dosages of 3 mg/kg of hIgG1, COM-902 analog, and urelumab are molar equivalent to 2.6 mg/kg and 1.6 mg/kg of ABL112 and parent anti-TIGIT sdAb, respectively. In the studies with mice, the researchers who conducted the experiments and analyzed the data were blinded to the drug types used. Mice were monitored two times per week, and there were no instances of unexpected death or clinical signs.

In the rechallenge study, mice that were cured from the treatment were monitored for ~3 months after cessation of antibody treatment. Cured mice from the urelumab (n=6) and ABL112 (n=6) groups were rechallenged with CT26 cells (5×10^5). Tumors were inoculated at the site opposite to that of the primary tumor challenge site. For the control group, six naïve mice with ages similar to those of the cured mice were challenged with CT26.

In a separate experiment, ABL112 efficacy was compared with the combination of each parent antibody. BALB/c-h4-1BB mice were subcutaneously injected with CT26 cells (5×10^5/0.1 mL/mouse) in the right flank. When tumor volume reached ~80 mm^3, mice were assigned to groups of eight and treated intraperitoneally two times per week for four doses with the following: hIgG1 (3 mg/kg), parent anti-TIGIT sdAb (1.6 mg/kg), combination of parent anti-TIGIT sdAb and parent anti-4-1BB mAb (1.6 mg/kg+3 mg/kg), and ABL112 (2.6 mg/kg). The dose levels were based on equal molar ratio.

To establish an H22 model, 6- to 8-week-old female BALB/c-h4-1BB mice were subcutaneously injected with H22 hepatoma cells (1×10^6 cells/0.1 mL/mouse) in the upper-right flank. When the mean tumor volume reached ~80 mm^3, mice were assigned to groups of five and treated intraperitoneally two times per week for a total of six times with the following: hIgG1 (7.5 mg/kg), parent anti-TIGIT sdAb (4 mg/kg), and ABL112 (6.65 mg/kg). The dosing volume was adjusted to the weight of the mouse (10 µL/g). The tumor volume and body weight were recorded two times per week.

For the rechallenge study, mice with complete regression (CR, cured mice) were monitored for ~3 months without antibody treatment. Mice were rechallenged with H22 cells (1×10^6). Five naive mice were used as controls.

In vivo immune cell depletion study

To assess immune cell depletion in the CT26 model, mice were assigned to their respective group consisting of eight mice per group when tumor volume reached ~80 mm^3 and administered intraperitoneally with depleting antibodies to reduce specific immune cell subpopulations the day before ABL112 administration. Immune cell depletion was achieved via intraperitoneal injection with 200 µg anti-mouse CD4 (clone GK1.5, Bio X Cell, Lebanon, New Hampshire, USA), 200 µg anti-mouse CD8a (clone 2.43, Bio X Cell), or 20 µL anti-mouse asialo GM1 (BioLegend,

San Diego, California, USA) according to the manufacturer's instructions. Briefly, anti-CD4- and anti-CD8-depleting antibodies were administered every 4 days, and anti-asialo GM1 antibody was administered every 5 days. To block FcγR-mediated activity, 200 µg anti-mouse CD16/32 (clone 2.4G2, Bio X Cell) and 200 µg anti-mouse CD16.2 (clone 9E9, Bio X Cell) were administered two times per week beginning the day before ABL112 administration. To assess the immune cell depletion or FcγR blockade status, 70 µL of peripheral blood were collected on the day before the first administration of ABL112 for FACS analysis. Peripheral blood was subjected to RBC lysis (Invitrogen, Waltham, Massachusetts, USA) for 12 min at room temperature in the dark and incubated with or without Fc-blocking reagent (BioLegend) for 10 min. The antibody cocktails in FACS buffer (PBS with 2 mM EDTA, 10 mM HEPES, and 2% FBS) were added at specific dilutions and incubated for 60 min in the dark as indicated by the manufacturer. Cells were washed three times with FACS buffer and resuspended in FACS buffer containing live/dead dye (Invitrogen). All the procedures were performed at 4°C. After confirming specific immune cell depletion, 2.6 mg/kg ABL112 was administered intraperitoneally two times per week for a total of seven times.

Peripheral and intra-tumoral immune cell analysis

For the detection of memory T cells, mouse peripheral blood was collected from age-matched naive (n=6) and cured mice (n=6) on days –7, 7, 14, and 28 of the rechallenge with CT26 and subjected to flow cytometry according to the manufacturer's protocol (BV510 anti-mouse CD45, AF700 anti-mouse CD3 (BioLegend), BV711 anti-mouse CD4 (BioLegend), BV605 anti-mouse CD62L (BioLegend), FITC anti-mouse CD8 (eBioscience, Waltham, Massachusetts, USA), P55 anti-mouse CD44 (BD Bioscience), and Ef780 live/dead dye (eBioscience). Immunofluorescence was measured using an Attune NxT Flow cytometer (Thermo, Waltham, Massachusetts, USA), and data were analyzed using FlowJo v10 software (FlowJo, Oregon, USA).

For intratumoral immune cell analysis, H22 tumors (seven mice per group) were dissociated with enzyme mix (RWD Life Science) for 60 min, filtered through a 70 µm strainer, treated with RBC lysis buffer (Invitrogen) for 3 min at room temperature in the dark, and resuspended in FACS buffer (PBS with 2 mM EDTA, 10 mM HEPES, and 2% FBS). Samples were incubated with live/dead dye (Invitrogen) for 10 min in the dark, washed, and blocked with Fc-blocking antibody (BioLegend) for 10 min. Cells were incubated with antibody cocktails in FACS buffer for 60 min, washed, and fixed with fixation/permeabilization buffer (eBioscience) for 50 min in the dark at 4°C.

Multiple antibodies for FACS analysis including BV605 anti-mouse CD45, AF700 anti-mouse CD3, APC-H7 anti-mouse CD4, PE-D594 anti-mouse CD335, P55 anti-mouse CD226, and BV650 anti-human CD137 (h4-1BB) were purchased from BioLegend. Other FACS antibodies included FITC antimouse CD8 (MBL, Nagoya, Japan), PE-CY7 anti-mouse CD25 (BD Bioscience, San Jose, California, USA), BV786 anti-mouse TIGIT (BD Bioscience), BV711 anti-mouse CD96 (BD Bioscience), and PE anti-mouse FOXP3 (eBioscience).

Reverse transcription-PCR

Tumors were cut into 20–50 mg pieces, and RNA was extracted using RNeasy Isolation Reagent (Vazyme, Nanjing, China) according to the manufacturer's instructions. RNA concentration was quantified using a Nanodrop system (Quawell, Sunnyvale, California, USA). OD260/OD280 was used for quality control of mRNA quality. An OD260/OD280 ratio of 1.8–2.2 was considered qualified. All mRNA samples used in the experiment were confirmed to qualify for this standard. Using the extracted RNA as template, cDNA was synthesized using a PrimeScript RT reagent Kit (Takara, Kusatsu, Japan) according to the manufacturer's instructions. Finally, qPCR was conducted using ChamQ Universal SYBR qPCR Master Mix (Vazyme). The PCR cycling conditions were as follows: an initial denaturation at 95°C for 30 s, followed by 40 cycles of denaturation at 95°C for 10 s, and annealing/extension at 60°C for 30 s. The primer sequences are listed in online supplemental table 1.

In vivo combination study

For the anti-PD-1 combination study, BALB/c-hPD-1/hPD-L1/hCD137 (h4-1BB) knock-in mice (BALB/cJGpt-Pdcd1$^{em1Cin(hPDCD1)}$Cd274$^{tm1(hCD274)}$Tnfrsf9$^{em1Cin(hTNFRSF9)}$/Gpt) were supplied by GemPharmatech. The female BALB/c-hPD-1/hPD-L1/h4-1BB mice (6–8 weeks old) were subcutaneously injected with CT26/hPD-L1 tumor cells (1×10^6/0.1 mL/mouse) in the lower right flank. When the tumor volume reached ~200 mm^3, mice were grouped (five mice per group) and intraperitoneally treated with 3 mg/kg hIgG1, 1.6 mg/kg parent anti-TIGIT sdAb, 2.6 mg/kg ABL112, 0.3 mg/kg pembrolizumab, 1.6 mg/kg parent anti-TIGIT sdAb+0.3 mg/kg pembrolizumab, or 2.6 mg/kg ABL112+0.3 mg/kg pembrolizumab two times per week for a total of six times. The tumor volume and body weight were recorded two times per week. The protocol and any amendments or procedures involving the care and use of animals in this experiment were reviewed and approved by the IACUC of GemPharmatech (GPTAP20230718-2).

For the anti-PD-L1 combination study, C57BL/6-h4-1BB/hTIGIT mice (C57BL/6-Tnfrsf9$^{tm1(TNFRSF9)}$ Tigit$^{tm1(TIGIT)}$/Bcgen) were supplied by Biocytogen (Beijing, China). Female C57BL/6-h4-1BB/hTIGIT mice (6–8 weeks old) were injected subcutaneously with MC38 tumor cells (5×10^5/0.1 mL/mouse) in the upper right flank. When tumor volume reached 100–150 mm^3, mice were grouped (five mice per group) and treated intraperitoneally with 3 mg/kg hIgG1, 0.3 mg/kg, 3 mg/kg ABL112, 3 mg/kg atezolizumab, 10 mg/kg tiragolumab, 0.3 mg/kg ABL112+3 mg/kg atezolizumab, or 10 mg/kg tiragolumab+3 mg/kg atezolizumab every 3 days for a total of six times. The tumor volume and body weight

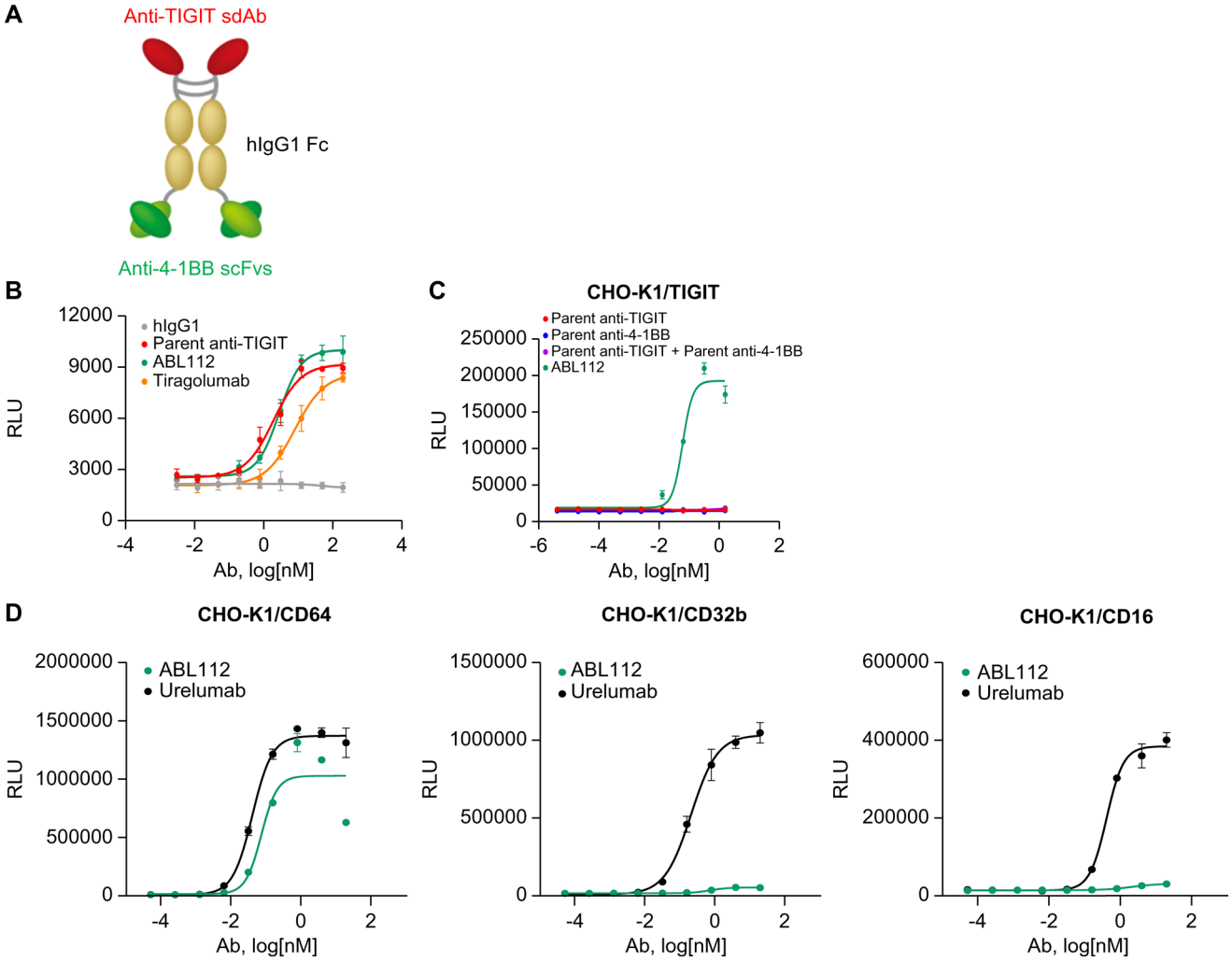

Figure 1 ABL112 blocks TIGIT–CD155-mediated T cell suppression and activates 4-1BB in a TIGIT- and FcγRI-dependent manner. (A) Schematic structure of ABL112. Anti-TIGIT single-domain antibodies (sdAbs) and anti-4-1BB single-chain fragment variables (scFvs) are linked to the hinge region and C-terminal ends by $(GS)_9$ linkers, respectively. (B) T cell restoration in TIGIT–CD155-mediated T cell suppression determined using luciferase reporter-expressing NF-κB-Luc2/CD226/TIGIT Jurkat T cells in the presence of CHO-K1/CD155-mimicking antigen-presenting cells. (C, D) 4-1BB activation determined using the luciferase reporter-expressing NF-κB-Luc2/4-1BB Jurkat T cells in the presence of CHO-K1 cells expressing TIGIT (C) or FcγR subtypes (D) including CD64, CD32b, and CD16a.

were recorded two times per week. The protocol and any amendments or procedures involving the care and use of animals in this experiment were reviewed and approved by the IACUC of Biocytogen (PS-01–2312053).

Statistical analyses

Statistical analyses were performed using GraphPad Prism V.10.0.1 (GraphPad Software Inc). For the in vivo experiments, a one-way or two-way analysis of variance (ANOVA) with Dunnett's multiple-comparison test or one-way ANOVA with Fisher's multiple-comparison (LSD) test was used. Survival was assessed using Kaplan-Meier survival curves. Significant differences in survival were calculated using the log-rank (Mantel-Cox) test. Statistical significances were indicated as *p<0.05, **p<0.01, ***p<0.001, and ****p<0.0001. Only statistically significant comparisons are marked.

Patient and public involvement

Not applicable.

RESULTS

Antibody structure and binding analysis of Fc-competent TIGITx4-1BB BsAb

ABL112, a novel TIGITx4-1BB BsAb, is composed of an anti-TIGIT sdAb, IgG_1 Fc, and anti-4-1BB scFv (figure 1A). The TIGIT sdAb was cloned to the N-terminal hinge region of CH_2 on the IgG_1 Fc region. Anti-4-1BB scFvs were cloned into the C-terminals of CH_3 through $(GS)_9$ linkers. Briefly, parental TIGIT sdAb and parental 4-1BB mAb were screened from the camel immune heavy chain and phage libraries, respectively. Anti-4-1BB antibodies were further screened for their dependency on target-mediated crosslinking for 4-1BB activation, that

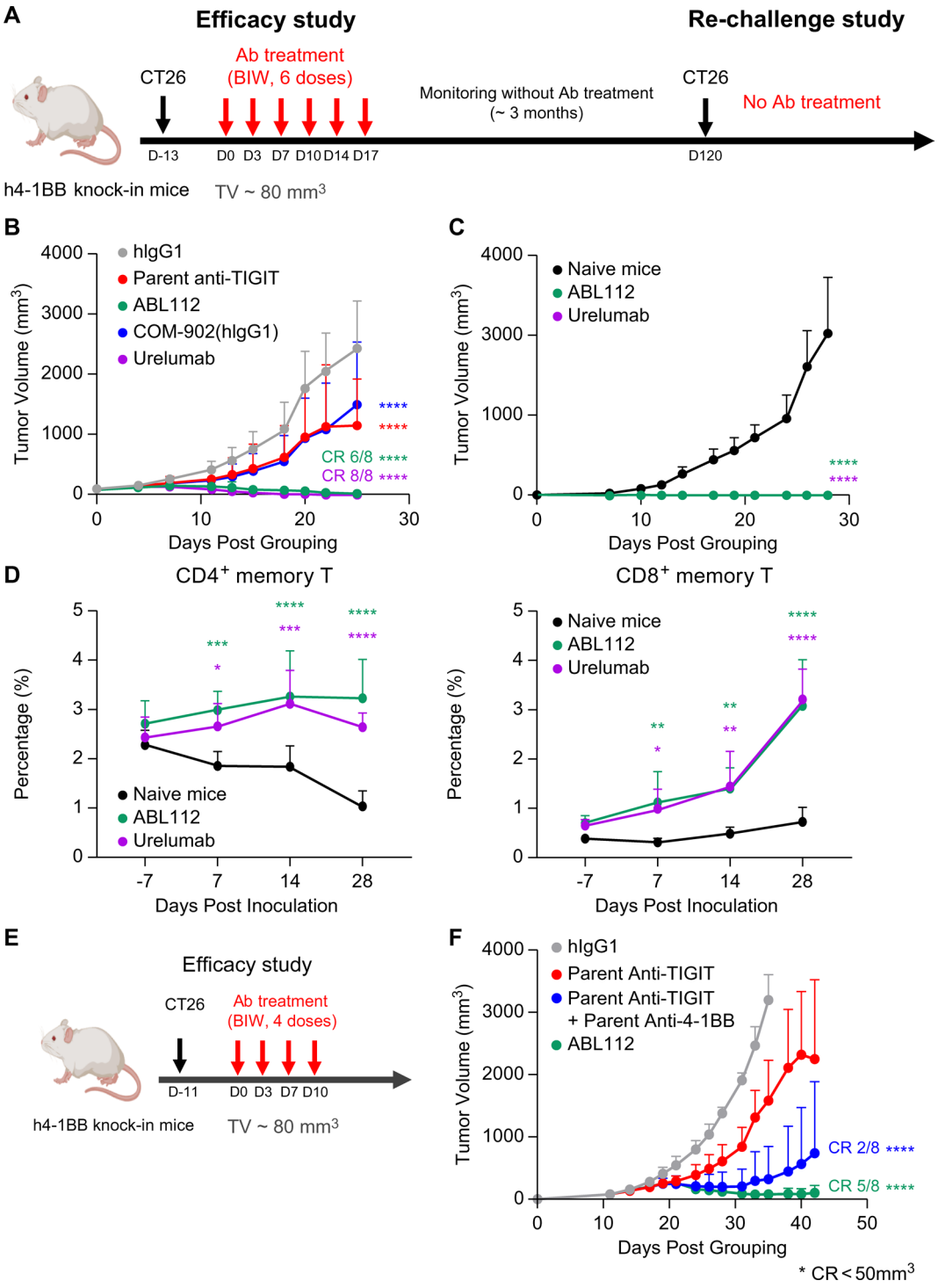

Figure 2 ABL112 strongly inhibits in vivo tumor progression compared with the combination of parent anti-TIGIT and anti-4-1BB antibodies and induces protective memory in CT26 mouse model. (A) Experimental workflow of ABL112 treatment in BALB/c h4-1BB knock-in mice subcutaneously engrafted with CT26 cells. (B) Tumor volumes, presented as the mean±SD. (C) Tumor volumes in rechallenged mice (n=6 mice per group). Naïve mice were used as positive controls. (B, C) Statistical analysis was performed using two-way analysis of variance with Dunnett's multiple-comparison test, with the hIgG1 group (B) and naive mice (C), designated respectively as the control group. (D) Proportions (mean±SD) of memory CD4$^+$ T and memory CD8$^+$ T cells determined by measuring CD44$^+$ T cell levels in each T cell subset. (E) Study scheme of ABL112 treatment. (F) Tumor growth inhibition. Tumor volumes are presented as the mean±SD. Statistical analysis was performed using Dunnett's multiple-comparison test, with hIgG1 group designated as the control group. *p<0.05, **p<0.01, ***p<0.001, ****p<0.0001.

is, conditional 4-1BB agonist; therefore, 4-1BB mAb by itself does not activate 4-1BB. In dual-antigen captured ELISA (online supplemental methods), ABL112 bound to TIGIT and 4-1BB simultaneously (EC_{50}: 0.3 nM; online supplemental figure 1B). ABL112 bound to Jurkat T and CHO-K1 cells expressing 4-1BB and TIGIT with an EC_{50} of

3.3 and 0.2 nM, respectively (online supplemental figure 1C,D). ABL112 showed lower 4-1BB-binding activity than urelumab (EC_{50}: 0.3 nM) but comparable binding activity to its parent anti-4-1BB antibody (EC_{50}: 2.6 nM) (online supplemental figure 1C). ABL112 bound to CHO-K1-expressing hTIGIT (EC_{50}: 0.2 nM) with comparable affinity to that of the parent anti-TIGIT sdAb (EC_{50}: 0.1 nM) (online supplemental figure 1D). ABL112 also bound to expanded Tregs (EC_{50}: 0.2 nM) with binding activity comparable to that of CHO-K1/TIGIT (online supplemental figure 1D,E). The analysis of tiragolumab (EC_{50}: 0.7 nM), parent anti-TIGIT sdAb (EC_{50}: 0.1 nM), and ABL112 showed that tiragolumab had lower binding activity than ABL112 (online supplemental figure 1D,E). Surface plasmon resonance analysis showed that ABL112 bound to TIGIT and 4-1BB with a K_D of 0.5×10^{-9} M and 4.5×10^{-9} M, respectively (online supplemental table 2). Interestingly, ABL112 bound to mouse TIGIT with a K_D of 0.5×10^{-9} M, supporting the successful establishment of the syngeneic mouse model for in vivo analysis (online supplemental table 2).

ABL112 blocks TIGIT-mediated T cell suppression and induces 4-1BB activation in a TIGIT- and FcγRI-dependent manner

In the TIGIT/CD155 blockade assay, luciferase reporter-expressing NF-κB-luc2/CD226/TIGIT Jurkat T cells were incubated with CHO-K1/CD155-mimicking antigen-presenting cells. Both ABL112 and parent anti-TIGIT antibody strongly inhibited TIGIT–CD155 interactions, restoring T cell activity (EC_{50}: 2.8 nM) compared with the tiragolumab treatment (EC_{50}: 8.1 nM; figure 1B). In the 4-1BB activation assay, CHO-K1 cells expressing TIGIT were incubated with Jurkat T cells expressing 4-1BB and the NF-κB-responding luciferase gene (NF-κB-Luc2/4-1BB Jurkat cell line). ABL112 activated 4-1BB in a TIGIT-dependent manner (EC_{50}: 0.1 nM; figure 1C) but not in the presence of mock CHO-K1 cells (data not shown). However, neither parent anti-TIGIT sdAb alone nor its combination with anti-4-1BB mAb induced 4-1BB activation. These results indicate that anti-4-1BB mAb alone does not oligomerize 4-1BB; crosslinking of TIGIT and 4-1BB is necessary for T-cell activation (figure 1C). The requirement of anti-4-1BB scFv crosslinking to a TAA for 4-1BB activation has also been reported for ABL503 and ABL111.[24 25]

Previously we used Fc-null IgG1 (N297A) to minimize FcγR-mediated activation with ragistomig (ABL503; PD-L1×4–1BB) and givastomig (ABL111; Claudin18.2×4–1BB). However, the TIGITx4-1BB BsAb was designed to retain FcγR-binding activity to maximize the efficacy of ABL112. We assumed that Fc-competent TIGITx4-1BB could induce FcγR- and TIGIT-dependent 4-1BB activation. To identify the main FcγR isotype interacting with the Fc region of TIGITx4-1BB leading to 4-1BB activation, CHO-K1 cells expressing FcγRI (CD64), FcγRIIb (CD32b), or FcγRIIIa (CD16a) were incubated with the luciferase reporter-expressing NF-κB-Luc2/4-1BB Jurkat T cells. ABL112 strongly induced 4-1BB activation only in the presence of FcγRI-expressing CHO-K1 cells (figure 1D). This in vitro study indicated that ABL112 activates T cells in TIGIT- and FcγRI-dependent manners and blocks TIGIT-mediated T cell suppression.

ABL112 demonstrates stronger in vivo antitumor efficacy than the combination of parent anti-TIGIT and anti-4-1BB antibodies and protects mice from the rechallenge, supporting the establishment of immune memory

We compared the tumor inhibitory activity of ABL112 with that of urelumab and mouse TIGIT cross-reactive benchmark antibody, COM-902 analog.[26] IgG1 form of COM-902 analog was used for direct comparison with ABL112. Human 4-1BB knock-in mice were inoculated with CT26 and administered with antibodies when tumor volume reached ~80 mm^3. While ABL112 (2.6 mg/kg) strongly inhibited tumor growth, the molar equivalent doses of the COM-902 analog (3 mg/kg) and parent anti-TIGIT sdAb (1.6 mg/kg) only showed moderate inhibition (figure 2B). This suggests that blocking TIGIT alone is insufficient for complete tumor regression. Urelumab (3 mg/kg) also potently inhibited tumor progression, indicating that 4-1BB stimulation plays an essential role in tumor growth inhibition. ABL112 treatment resulted in complete tumor regression in six out of eight mice and its activity lasted for 100 days after discontinuation. In the rechallenge experiment, cured mice treated with both ABL112 and urelumab were protected from secondary tumor development (figure 2C). Peripheral blood mononuclear cells were harvested on days –7, 7, 14, and 28 after tumor rechallenge and analyzed for memory T cell levels. Cured mice showed increased proportions of memory $CD4^+$ ($CD4^+CD44^+$) and $CD8^+$ T cells ($CD8^+CD44^+$) at 7–28 days (figure 2D), reflecting the role of ABL112 in establishing immune memory.

In a separate experiment, we demonstrated that ABL112 (2.6 mg/kg) showed stronger tumor inhibitory activity compared with the combination of parent anti-TIGIT sdAb (1.6 mg/kg) and parent anti-4-1BB antibodies (3 mg/kg). This supports that crosslinking of TIGIT and 4-1BB endows additional antitumor activity compared with the combination of each parent mAb.

$CD8^+$ T cells and Fc-mediated activity are essential for the antitumor activity of ABL112

We investigated the mechanisms underlying the antitumor effects of ABL112 in tumor-bearing mice treated with ABL112 (2.6 mg/kg) in the presence of T cell- and NK cell-depleting antibodies or FcγR blockers (anti-mCD16/32 and anti-mCD16.2). Depletion of each immune cell subsets was confirmed by flow cytometry before ABL112 administration (online supplemental figure 2A). While specific immune cell subsets including $CD4^+$, $CD8^+$ T, and NK cells were depleted, there was no significant change in the total $mCD45^+$ and macrophage populations. The

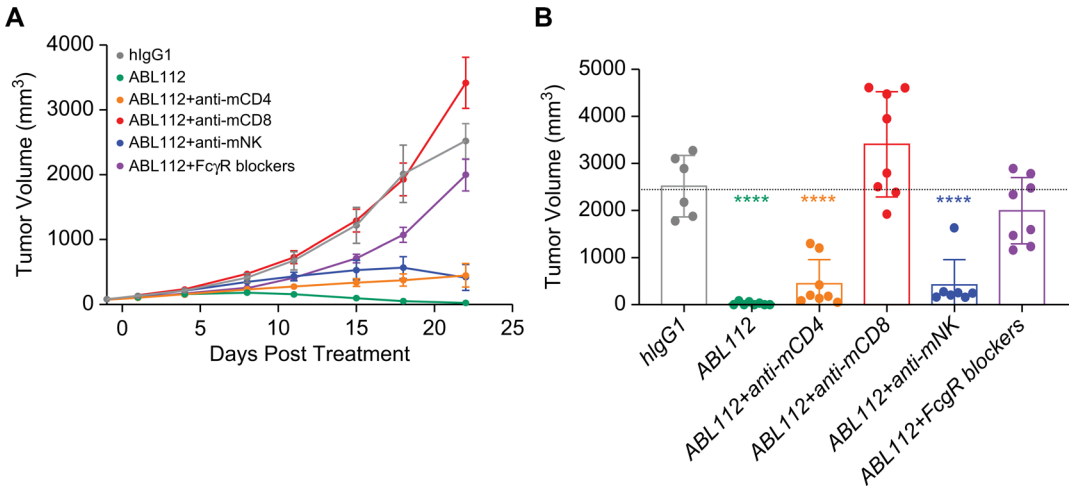

Figure 3 CD8$^+$ T cells play a major role in ABL112-mediated tumor suppression, followed by the FcγR-mediated activation. (A) Tumor volumes in BALB/c h4-1BB knock-in mice. After confirming depletion of specific immune cell subsets or blockade of FcγR, ABL112 was administered intraperitoneally two times per week. (B) Tumor volume on day 22. Statistical analysis was performed using two-way analysis of variance with Dunnett's multiple-comparison test, with the hIgG1 group designated as the control group. *p<0.05, **p<0.01, ***p<0.001, ****p<0.0001.

proportions of mCD16$^+$ or mCD32$^+$ NK cells and macrophages were partially reduced after treatment with FcγR-blocking antibodies, indicating partial blockade of these receptors. The tumor suppressive activity of ABL112 was mostly abolished by CD8-depleting antibodies and mCD16 and mCD32 blockers, implicating the essential roles of CD8$^+$ T cells and FcγR-dependent responses such as ADCC or ADCP (figure 3A,B). A substantial degree of tumor growth inhibition was still observed under NK or CD4$^+$ T cell depletion, suggesting that NK and CD4$^+$ T cells are not critical for the antitumor activity of ABL112. Therefore, monocyte/macrophage-mediated ADCP may be more important than NK cell-mediated ADCC activity. We could not determine the role of macrophages in tumor regression due to serious side effects leading to death after administration of clodronate liposome (data not shown). These findings suggested that CD8$^+$ T cells and FcγR-mediated activities play pivotal roles in the anti-tumor activity of ABL112.

ABL112 inhibits the growth of CD155-overexpressing H22 murine hepatoma by modulating the TME

In another mouse model with murine H22 hepatoma expressing high levels of endogenous CD155,[27] both the parent anti-TIGIT sdAb (4 mg/kg) (schematic structure shown in online supplemental figure 1A) and ABL112 (6.65 mg/kg) exerted robust antitumor activities; however, tumors relapsed around day 30 shortly after discontinuation of parent anti-TIGIT sdAb (figure 4B), indicating that, although TIGIT mAb monotherapy showed marked inhibition of tumor growth, its antitumor effects were ephemeral. This inhibitory efficacy of anti-TIGIT mAbs, such as parent anti-TIGIT sdAb and tiragolumab, was not observed in other tumor models, including the CT26 and MC38 models (figures 2B, 5A,B). Because H22 overexpresses CD155, it is likely that the blockade of TIGIT–CD155 interactions initially promoted tumor regression, but TIGIT blockade and Fc-mediated NK cell activation may not sustain long-term effects. In contrast, ABL112 (TIGITx4-1BB BsAb) strongly inhibited tumor growth with CR in all mice for up to 100 days. As observed in the CT26 model (figure 2C), cured H22 model mice were also protected from secondary tumor development (figure 4C).

To understand the mechanisms of action, BALB/c h4-1BB knock-in mice bearing H22 hepatoma were sacrificed 4 days after administration of ABL112 (6.65 mg/kg) and parent anti-TIGIT sdAb (4 mg/kg) on days 0 and 3, and tumors were harvested for flow cytometry and RT-PCR analysis. Parent anti-TIGIT sdAb and ABL112 induced the infiltration of CD8$^+$ and CD4$^+$ T cells (figure 4D). Interestingly, Treg depletion was only observed in ABL112-treated mice, which showed an increased CD8$^+$ T cell/Treg ratio. It was reported that 4-1BB is predominantly expressed in intratumoral Tregs compared with peripheral Tregs and other immune cells.[28] Similarly, we observed a 15-fold higher expression of 4-1BB in intratumoral Tregs compared with other intratumoral immune cells, such as CD8$^+$ T and NK cells. TIGIT expression in Tregs was approximately two fold higher than that in CD8$^+$ and NK cells (online supplemental figure 3C). Importantly, there was no decrease in intratumoral CD8$^+$ T or CD4$^+$ T cell numbers. Mouse CD226 as well as CD96 expression were induced after ABL112 treatment, suggesting that CD226-mediated stimulatory signaling may promote T cell activation under TIGIT blockade. We hypothesized that the ABL112-mediated crosslinking of TIGIT or 4-1BB to FcγR may proactively trigger FcγR activation. Based on the macrophage activation signatures, ABL112 significantly induced CXCL10, CXCL11, IFN-γ, and TNF-α expression, indicating FcγR-mediated myeloid cell activation (figure 4E).

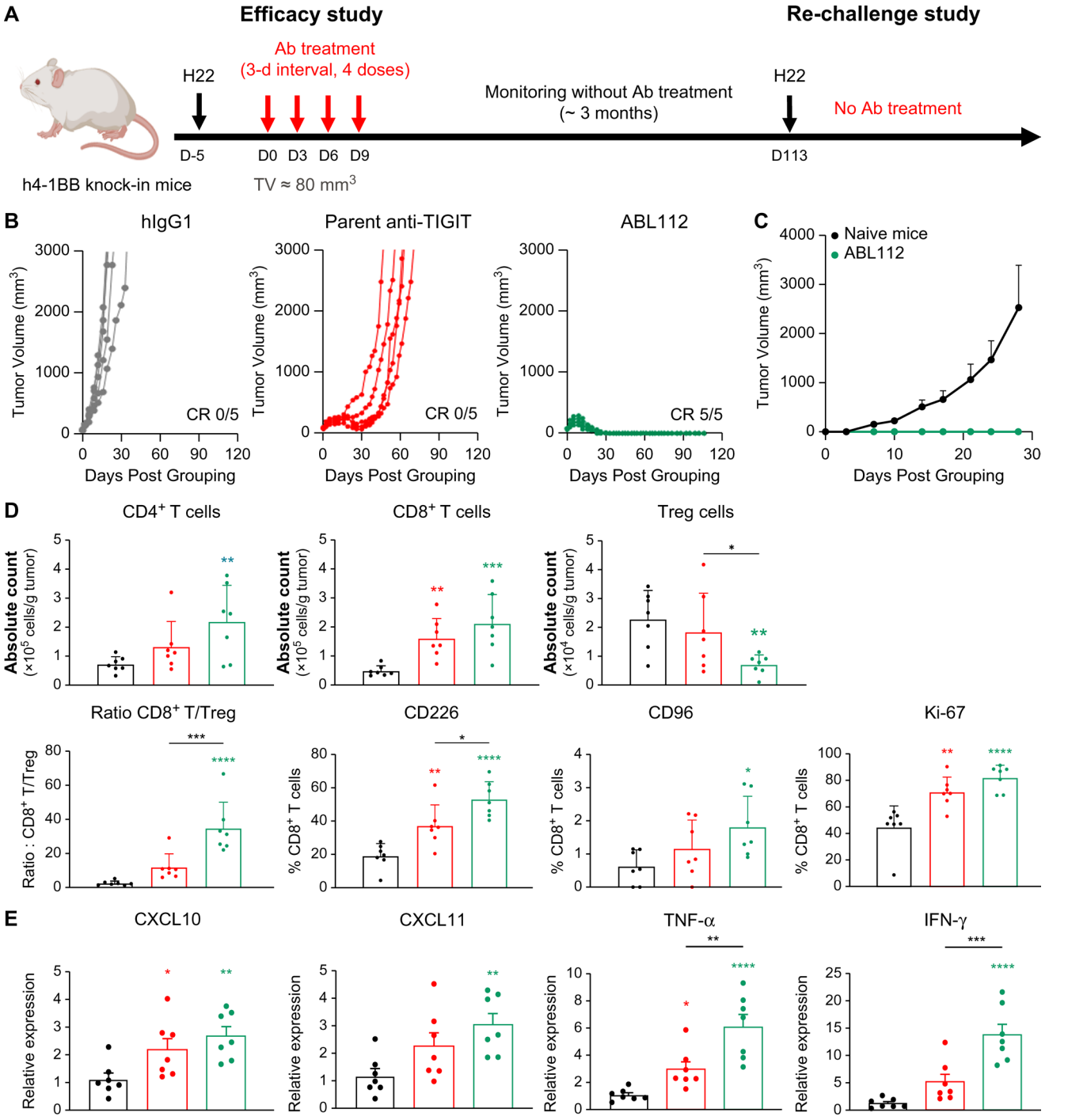

Figure 4 ABL112 strongly inhibits tumor progression and modulates the tumor microenvironment (TME) by promoting immune cell infiltration, Treg depletion, and myeloid cell activation in H22 hepatoma mouse model. (A) Experimental scheme of ABL112 treatment in BALB/c h4-1BB knock-in mice engrafted with H22 tumors for primary and secondary tumor challenges. (B) Individual tumor growth (n=5 mice per group). CR, complete regression (tumor volume<50 mm^3). (C) Tumor growth after tumor rechallenge (n=5 mice per group). Naïve mice were used as a positive control for H22 tumor progression. (D, E) Tumor-infiltrating lymphocyte (TIL) and qRT-PCR analyses in H22-tumor-engrafted BALB/c h4-1BB knock-in mice treated with ABL112 on days 0 and 3 (n=7 mice per group). Tumors were harvested and analyzed 4 days after the second administration. Black: hIgG1, Red: parent anti-TIGIT, Green: ABL112 (D) Flow cytometric analysis of TILs (absolute count (cell count per gram of tumor) and proportion). TILs were harvested, and absolute count of $CD4^+$ T, $CD8^+$ T, and Treg cells were determined. $CD8^+$ T/Treg cell ratio calculated by dividing the absolute counts for $CD8^+$ T cells by those for Treg cells. Proportions of $CD226^+$ or $CD96^+$ T cells within the $CD8^+$ T cell subsets are displayed. (E) Relative gene expression ($2^{-\Delta\Delta Ct}$); CXCL10, CXCL11, TNF-α, and IFN-γ expression based on RT-PCR. Data are representative of two independent experiments and presented as the mean±SEM. Statistical analysis was performed using one-way analysis of variance with Fisher's multiple-comparison (LSD) test, with the hIgG1 group designated as the control group. *p<0.05, **p<0.01, ***p<0.001, ****p<0.0001.

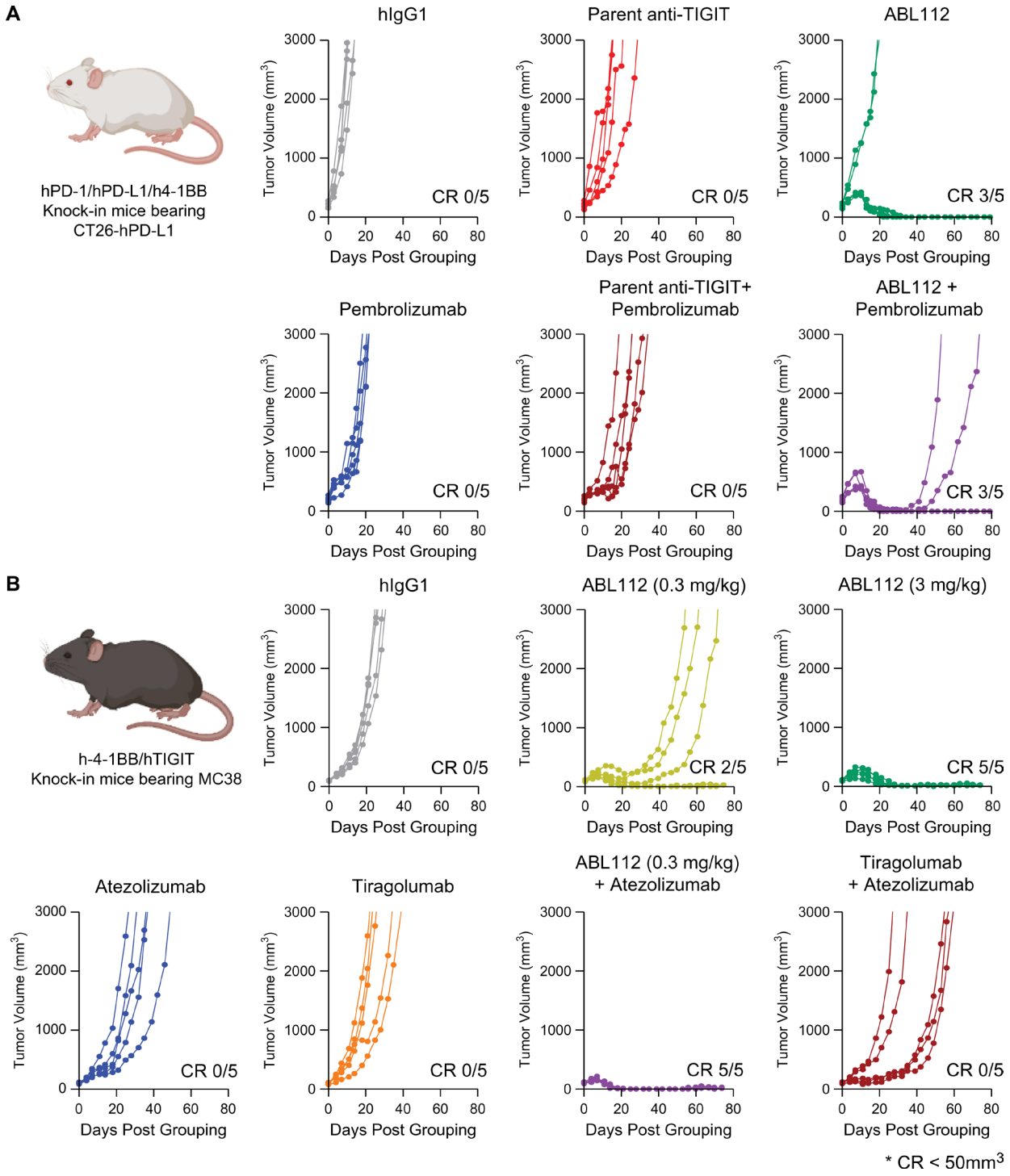

Figure 5 Combination of ABL112 with anti-PD-(L)1 synergistically inhibits tumor growth in two mouse models. (A) hPD-1/hPD-L1/h4-1BB knock-in BALB/c mice engrafted with CT26-hPD-L1 were treated with indicated antibodies (n=5 mice per group) two times per week for a total of six times. Tumor growth was measured two times per week for 80 days. Individual tumor growth is displayed. CR, complete regression (tumor volume<50 mm^3). (B) h4-1BB/hTIGIT knock-in mice engrafted with MC38 were treated with the indicated antibodies (n=5 per group) in a 3-day interval for a total of six times. Mice were euthanized when tumor volume reached ~3000 mm^3.

Combined ABL112–anti-PD-(L)1 treatment synergistically inhibits tumor growth, resulting in more potent tumor growth inhibition compared with anti-TIGIT–anti-PD-(L)1 combination

PD-1/PD-L1 blockades are the most extensively studied ICIs and co-inhibition of TIGIT and PD-1/PD-L1 represents a promising cancer treatment strategy.[5] Although co-inhibition of TIGIT and PD-1/PD-L1 enhanced antitumor immunity and treatment outcomes in preclinical and clinical studies, the response rates were insufficient potentially owing to the activities of Tregs and myeloid-derived suppressor cells.[3 6] To confirm the superior anticancer performance of ABL112 over anti-TIGIT

antibody, we tested the combined efficacies of ABL112–anti-PD-(L)1 antibody versus anti-TIGIT–anti-PD-(L)1 treatment. Triple hPD-1/hPD-L1/h4-1BB knock-in mice were inoculated with CT26-PD-L1 and treated with specific antibodies intraperitoneally two times per week (online supplemental figure 4A). The parent anti-TIGIT (1.6 mg/kg)–pembrolizumab (0.3 mg/kg) combination and antibody monotherapies showed moderate antitumor efficacy (figure 5A). However, ABL112 (2.6 mg/kg) showed better tumor growth inhibition, with complete tumor regression in three out of five mice. The ABL112–pembrolizumab combination initially prevented tumor growth in all mice, though tumor recurrence was observed in two mice (figure 5A and online supplemental figure 4A).

We confirmed the performance of the combination synergy in MC38-inoculated h4-1BB/hTIGIT knock-in mice. ABL112 exhibited dose-dependent tumor growth inhibition, with complete tumor regression in the 3 mg/kg group, while 10 mg/kg of tiragolumab failed to inhibit tumor progression (figure 5B). Atezolizumab (3 mg/kg), which binds to mouse PD-L1, did not inhibit tumor progression. However, a combination of low-dose ABL112 (0.3 mg/kg) and atezolizumab (3 mg/kg) showed synergistic antitumor efficacy, resulting in CR of tumors in all mice, unlike the tiragolumab–atezolizumab combination (figure 5B and online supplemental figure 4B). These findings suggested that ABL112 exerted potent antitumor activity through TIGIT inhibition and 4-1BB activation and represents a more promising therapeutic option in combination with anti-PD-(L)1 therapies.

DISCUSSION

ICIs have emerged as key anticancer agents with substantial survival benefits in clinical practice. However, patient response rates vary across cancers, and a significant proportion of patients experience relapse or nonresponsive tumor progression.[29–32] Therefore, dual ICI combination therapy, such as PD-(L)1 plus anti-TIGIT antibody, may potentiate the required antitumor immune response. Preclinical studies have demonstrated that the combination of TIGIT and PD-1/PD-L1 resulted in better antitumor efficacy.[5 6 33] However, multiple clinical trials on TIGIT and PD-1/PD-L1 combination therapy in various cancer types have shown limited success.[34]

To address the limitations of combined TIGIT–PD-(L)1 therapies, we hypothesized that leveraging 4-1BB for Treg depletion and $CD8^+$ T cell activation could effectively enhance intratumoral immunity. ABL112 restored T cell activity by abolishing TIGIT–CD155 interactions and activating 4-1BB in a TIGIT- and CD64-dependent manner. In vivo, we also observed high levels of $CD8^+$ T cell tumor infiltration. Incorporation of a competent Fc within the ABL112 backbone structure may enable bidirectional activation of 4-1BB and FcγR. This is consistent with our in vivo study showing increased $CD8^+$ T cell proliferation and myeloid activation, as indicated by the increased levels of inflammatory cytokines and chemokines, including CXCL10, CXCL11, TNF-α, and IFN-γ. Moreover, a marked decrease in intratumoral Treg levels was observed, whereas there was no decrease in intratumoral CD8 T cell levels, reflecting the intratumoral Treg-specific performance of ABL112 in vivo.

Tregs inhibit T cell activation and promote the establishment of an immunosuppressive TME by competing with effector T cells for IL-2, secreting immunosuppressive cytokines such as TGF-β and IL-10, and triggering immune checkpoint-mediated T cell suppression.[35 36] Given their T cell inhibitory role, Tregs emerged as an appealing target in antitumor therapies. To maximize antitumor activity and avoid systemic toxicity, such as autoimmune disease, it is critical that only intratumoral Treg cells are depleted but not peripheral Tregs or other intratumoral T cell subsets. The targeting of CCR4, a Treg biomarker, using the anti-CCR4 antibody mogamulizumab showed minimal clinical efficacy likely owing to the concurrent depletion of central memory $CD8^+$ T cells.[37] Freeman *et al* reported that 4-1BB is one of the most highly expressed markers in intratumoral Tregs but not in peripheral Tregs.[28] In a CT26 tumor mouse model, ADCC-competent IgG2a anti-4-1BB mouse antibody depleted intratumoral Tregs but not Tregs or CD8 T cells in the spleen.[28] The ICIs CTLA-4 and OX40 are also overexpressed in intratumoral Tregs; however, anti-CTLA-4 and anti-OX40 mAb treatment increased and decreased splenic Treg levels, respectively, indicating their limited suitability as Treg targets.[28] In our study, 4-1BB expression in intratumoral Tregs was ~15-fold higher than that of the other immune cell subsets, such as $CD8^+$ T and NK cells. Consistent with the change in 4-1BB expression, we observed the depletion of Tregs but not $CD4^+$ or $CD8^+$ T cells.

We found that 4-1BB was activated in the presence of CHO-K1 cells expressing CD64 (FcγRI) but not CD32b (FcγRIIb) or CD16a (FcγRIIIa). Human IgG1 shows the strongest binding to FcγRI followed by FcγRII and FcγRIII, suggesting that a certain level of binding affinity is required for inducing 4-1BB activation.[38] In the immune cell depletion/blockade study, CD16/32 blockade reverted the ABL112-mediated tumor regression, suggesting that FcγRII/III-mediated ADCC or ADCP plays a pivotal role, despite the lack of FcγRII/III-dependent 4-1BB activation. In contrast, NK cell depletion only had minor effects on tumor regression. This suggested that macrophage-mediated ADCP rather than NK cell-mediated ADCC facilitated tumor regression in the CT26 tumor model. One limitation of this study is the absence of CD64 blockade, preventing a full understanding of the impact of CD64-mediated activities, such as CD64-dependent 4-1BB activation and CD64-mediated ADCP, on tumor suppression.

Although anti-TIGIT mAb did not demonstrate robust antitumor activities in most of the tumor models, it showed potent but short-lived tumor suppressive activity in the CD155-overexpressing H22 hepatoma model.[27]

The higher expression of CD155 in H22 compared with CT26 or MC38 cells suggests that the TIGIT–CD155 axis may be crucial for tumor progression in certain tumors such as hepatocellular carcinoma. In this regard, it is interesting that the combination of tiragolumab with atezolizumab and bevacizumab showed greater efficacy than the atezolizumab/bevacizumab arm in phase Ib/II MORPHEUS-Liver.[39] Poor prognosis was also observed in CD155-high patients with hepatocellular carcinoma.[40] CD155 expression was associated with poor prognosis in a broad range of cancers, including lung cancer,[41–43] cholangiocarcinoma,[44] and breast cancer.[45 46] CD155 expression was prevalent in several hematological cancers, including acute myeloid leukemia and multiple myeloma, and associated with worse prognosis.[47] This suggests that ABL112 may exert antitumor effects in hematological as well as in solid tumors.

It would be intriguing to track the longitudinal TME changes to understand potent long-lived efficacy of ABL112 alone or in combination with PD-(L)1 antibodies. Such studies could provide clues for resolving the moderate clinical outcomes of anti-TIGIT antibodies.

In conclusion, ABL112 exerted its anticancer effects via multiple mechanism of action. ABL112 induced TIGIT- and FcγRI-dependent 4-1BB activation and restored T cell activity through TIGIT/CD155 blockade. 4-1BB and TIGIT were overexpressed in Treg cells; therefore, cross-linking of 4-1BB/TIGIT and FcγR potentially mediated proactive FcγR signaling, myeloid activation, and cell-mediated Treg depletion through ADCC and ADCP (online supplemental figure 5).

Acknowledgements We would like to acknowledge Editage's (http://www.editage.cn) support in manuscript preparation.

Contributors Study conceptualization and design: YL, JW. Antibody production: HY. Antibody purification and SPR analysis: AS, BS. In vitro study: WS, YP, KP, SK. Animal study design, analysis, and interpretation: WS, YP, KP, SK, YL, JW. Writing and review of the manuscript: WS, YL, SHL, JW. Guarantor of the study: JW.

Funding This work was supported by a grant from ABL Bio Inc., Republic of Korea.

Competing interests WS, YL, YP, KP, SK, HY, AS, BS, and JW are employees of ABL Bio, Inc. SHL is the CEO of ABL Bio, Inc.

Patient consent for publication Not applicable.

Ethics approval The animal protocols were reviewed and approved by the Institutional Animal Care and Use Committees of GemPharmatech (GPTAP20221010-6/GPTAP20230214-2/GPTAP20230627-4/GPTAP20231030-2/GPTAP20230718-2) and Biocytogen (PS-01-2312053).

Provenance and peer review Not commissioned; externally peer reviewed.

Data availability statement All data relevant to the study are included in the article or uploaded as supplementary information.

ORCID iD

Jonghwa Won http://orcid.org/0000-0003-2853-8948

REFERENCES

1 Yu X, Harden K, Gonzalez LC, *et al*. The surface protein TIGIT suppresses T cell activation by promoting the generation of mature immunoregulatory dendritic cells. *Nat Immunol* 2009;10:48–57.
2 Manieri NA, Chiang EY, Grogan JL. TIGIT: A Key Inhibitor of the Cancer Immunity Cycle. *Trends Immunol* 2017;38:20–8.
3 Chiang EY, Mellman I. TIGIT-CD226-PVR axis: advancing immune checkpoint blockade for cancer immunotherapy. *J Immunother Cancer* 2022;10:e004711.
4 Stengel KF, Harden-Bowles K, Yu X, *et al*. Structure of TIGIT immunoreceptor bound to poliovirus receptor reveals a cell-cell adhesion and signaling mechanism that requires cis-trans receptor clustering. *Proc Natl Acad Sci U S A* 2012;109:5399–404.
5 Chauvin JM, Zarour HM. TIGIT in cancer immunotherapy. *J Immunother Cancer* 2020;8:e000957.
6 Chu X, Tian W, Wang Z, *et al*. Co-inhibition of TIGIT and PD-1/PD-L1 in Cancer Immunotherapy: Mechanisms and Clinical Trials. *Mol Cancer* 2023;22:93.
7 Rousseau A, Parisi C, Barlesi F. Anti-TIGIT therapies for solid tumors: a systematic review. *ESMO Open* 2023;8:101184.
8 Cho BC, Abreu DR, Hussein M, *et al*. Tiragolumab plus atezolizumab versus placebo plus atezolizumab as a first-line treatment for PD-L1-selected non-small-cell lung cancer (CITYSCAPE): primary and follow-up analyses of a randomised, double-blind, phase 2 study. *Lancet Oncol* 2022;23:781–92.
9 Guan X, Hu R, Choi Y, *et al*. Anti-TIGIT antibody improves PD-L1 blockade through myeloid and T_{reg} cells. *Nature New Biol* 2024;627:646–55.
10 Han J-H, Cai M, Grein J, *et al*. Effective Anti-tumor Response by TIGIT Blockade Associated With FcγR Engagement and Myeloid Cell Activation. *Front Immunol* 2020;11:573405.
11 Johnson ML, Fox W, Lee Y-G, *et al*. ARC-7: Randomized phase 2 study of domvanalimab + zimberelimab ± etrumadenant versus zimberelimab in first-line, metastatic, PD-L1-high non-small cell lung cancer (NSCLC). *JCO* 2022;40:397600.
12 Janjigian YY, Oh D-Y, Pelster M, *et al*. EDGE-Gastric Arm A1: Phase 2 study of domvanalimab, zimberelimab, and FOLFOX in first-line (1L) advanced gastroesophageal cancer. *JCO* 2023;41:433248.
13 So T, Lee SW, Croft M. Tumor necrosis factor/tumor necrosis factor receptor family members that positively regulate immunity. *Int J Hematol* 2006;83:1–11.
14 Wyzgol A, Müller N, Fick A, *et al*. Trimer stabilization, oligomerization, and antibody-mediated cell surface immobilization improve the activity of soluble trimers of CD27L, CD40L, 41BBL, and glucocorticoid-induced TNF receptor ligand. *J Immunol* 2009;183:1851–61.
15 Chester C, Sanmamed MF, Wang J, *et al*. Immunotherapy targeting 4-1BB: mechanistic rationale, clinical results, and future strategies. *Blood* 2018;131:49–57.
16 Segal NH, Logan TF, Hodi FS, *et al*. Results from an Integrated Safety Analysis of Urelumab, an Agonist Anti-CD137 Monoclonal Antibody. *Clin Cancer Res* 2017;23:1929–36.
17 Segal NH, He AR, Doi T, *et al*. Phase I Study of Single-Agent Utomilumab (PF-05082566), a 4-1BB/CD137 Agonist, in Patients with Advanced Cancer. *Clin Cancer Res* 2018;24:1816–23.
18 Eskiocak U, Guzman W, Wolf B, *et al*. Differentiated agonistic antibody targeting CD137 eradicates large tumors without hepatotoxicity. *JCI Insight* 2020;5:e133647.
19 Ma Y, Luo F, Zhang Y, *et al*. Preclinical characterization and phase 1 results of ADG106 in patients with advanced solid tumors and non-Hodgkin's lymphoma. *Cell Rep Med* 2024;5:101414.
20 Kamata-Sakurai M, Narita Y, Hori Y, *et al*. Antibody to CD137 Activated by Extracellular Adenosine Triphosphate Is Tumor Selective and Broadly Effective *In Vivo* without Systemic Immune Activation. *Cancer Discov* 2021;11:158–75.
21 Narita Y, Kamata-Sakurai M. 578 Tumor selective immune responses of sta551, a novel anti-cd137 agonist antibody activated by extracellular atp. *J Immunother Cancer* 2020;8 Suppl 3:A346–AA7.
22 Galand C, Venkatraman V, Marques M, *et al*. 377 AGEN2373 is a cd137 agonist antibody designed to leverage optimal cd137 and fcγr

co-targeting to promote antitumor immunologic effects. *J Immunother Cancer* 2020;8 Suppl 3:A229–AA30.
23 Claus C, Ferrara-Koller C, Klein C. The emerging landscape of novel 4-1BB (CD137) agonistic drugs for cancer immunotherapy. *MAbs* 2023;15:2167189.
24 Jeong S, Park E, Kim H-D, *et al*. Novel anti-4-1BB×PD-L1 bispecific antibody augments anti-tumor immunity through tumor-directed T-cell activation and checkpoint blockade. *J Immunother Cancer* 2021;9:e002428.
25 Gao J, Wang Z, Jiang W, *et al*. CLDN18.2 and 4-1BB bispecific antibody givastomig exerts antitumor activity through CLDN18.2-expressing tumor-directed T-cell activation. *J Immunother Cancer* 2023;11:e006704.
26 Hansen K, Kumar S, Logronio K, *et al*. COM902, a novel therapeutic antibody targeting TIGIT augments anti-tumor T cell function in combination with PVRIG or PD-1 pathway blockade. *Cancer Immunol Immunother* 2021;70:3525–40.
27 Zuo S, Wei M, He B, *et al*. Enhanced antitumor efficacy of a novel oncolytic vaccinia virus encoding a fully monoclonal antibody against T-cell immunoglobulin and ITIM domain (TIGIT). *EBioMedicine* 2021;64:103240.
28 Freeman ZT, Nirschl TR, Hovelson DH, *et al*. A conserved intratumoral regulatory T cell signature identifies 4-1BB as a pan-cancer target. *J Clin Invest* 2020;130:1405–16.
29 Das S, Johnson DB. Immune-related adverse events and anti-tumor efficacy of immune checkpoint inhibitors. *J Immunother Cancer* 2019;7:306.
30 Wang B, Han Y, Zhang Y, *et al*. Overcoming acquired resistance to cancer immune checkpoint therapy: potential strategies based on molecular mechanisms. *Cell Biosci* 2023;13:120.
31 Walsh RJ, Sundar R, Lim JSJ. Immune checkpoint inhibitor combinations-current and emerging strategies. *Br J Cancer* 2023;128:1415–7.
32 Hiltbrunner S, Cords L, Kasser S, *et al*. Acquired resistance to anti-PD1 therapy in patients with NSCLC associates with immunosuppressive T cell phenotype. *Nat Commun* 2023;14:5154.
33 Ge Z, Peppelenbosch MP, Sprengers D, *et al*. TIGIT, the Next Step Towards Successful Combination Immune Checkpoint Therapy in Cancer. *Front Immunol* 2021;12:699895.
34 Zhang P, Liu X, Gu Z, *et al*. Targeting TIGIT for cancer immunotherapy: recent advances and future directions. *Biomark Res* 2024;12:7.
35 Li C, Jiang P, Wei S, *et al*. Regulatory T cells in tumor microenvironment: new mechanisms, potential therapeutic strategies and future prospects. *Mol Cancer* 2020;19:116.
36 Scott EN, Gocher AM, Workman CJ, *et al*. Regulatory T Cells: Barriers of Immune Infiltration Into the Tumor Microenvironment. *Front Immunol* 2021;12:702726.
37 Maeda Y, Wada H, Sugiyama D, *et al*. Depletion of central memory $CD8^+$ T cells might impede the antitumor therapeutic effect of Mogamulizumab. *Nat Commun* 2021;12:7280.
38 Bruhns P, Iannascoli B, England P, *et al*. Specificity and affinity of human Fcgamma receptors and their polymorphic variants for human IgG subclasses. *Blood* 2009;113:3716–25.
39 Finn RS, Ryoo B-Y, Hsu C-H, *et al*. Results from the MORPHEUS-liver study: Phase Ib/II randomized evaluation of tiragolumab (tira) in combination with atezolizumab (atezo) and bevacizumab (bev) in patients with unresectable, locally advanced or metastatic hepatocellular carcinoma (uHCC). *JCO* 2023;41:4010.
40 Liu W-F, Quan B, Li M, *et al*. PVR-A Prognostic Biomarker Correlated with Immune Cell Infiltration in Hepatocellular Carcinoma. *Diagnostics (Basel)* 2022;12:2953.
41 Xu Y, Cui G, Jiang Z, *et al*. Survival analysis with regard to PD-L1 and CD155 expression in human small cell lung cancer and a comparison with associated receptors. *Oncol Lett* 2019;17:2960–8.
42 Oyama R, Kanayama M, Mori M, *et al*. CD155 expression and its clinical significance in non-small cell lung cancer. *Oncol Lett* 2022;23:166.
43 Sun Y, Luo J, Chen Y, *et al*. Combined evaluation of the expression status of CD155 and TIGIT plays an important role in the prognosis of LUAD (lung adenocarcinoma). *Int Immunopharmacol* 2020;80:106198.
44 Huang DW, Huang M, Lin XS, *et al*. CD155 expression and its correlation with clinicopathologic characteristics, angiogenesis, and prognosis in human cholangiocarcinoma. *Onco Targets Ther* 2017;10:3817–25.
45 Yong H, Cheng R, Li X, *et al*. CD155 expression and its prognostic value in postoperative patients with breast cancer. *Biomed Pharmacother* 2019;115:108884.
46 Triki H, Charfi S, Bouzidi L, *et al*. CD155 expression in human breast cancer: Clinical significance and relevance to natural killer cell infiltration. *Life Sci* 2019;231:116543.
47 Lee B-H, Kim J-H, Kang K-W, *et al*. PVR (CD155) Expression as a Potential Prognostic Marker in Multiple Myeloma. *Biomedicines* 2022;10:1099.